MOLECULAR AND CELLULAR BIOLOGY, Dec. 2010, p. 5572–5581 Vol. 30, No. 23
0270-7306/10/$12.00 doi:10.1128/MCB.00917-10

Dual Functions of Nbs1 in the Repair of DNA Breaks and Proliferation Ensure Proper V(D)J Recombination and T-Cell Development▽†

Amal Saidi,[1]# Tangliang Li,[1]# Falk Weih,[1,2] Patrick Concannon,[3] and Zhao-Qi Wang[1,2]*

Leibniz Institute for Age Research-Fritz Lipmann Institute (FLI)[1] and Faculty of Biology and Pharmacy, Friedrich Schiller University of Jena,[2] Jena, Germany, and Department of Biochemistry and Molecular Genetics and Center for Public Health Genomics, University of Virginia, Charlottesville, Virginia[3]

Received 7 August 2010/Returned for modification 14 September 2010/Accepted 21 September 2010

Immunodeficiency and lymphoid malignancy are hallmarks of the human disease Nijmegen breakage syndrome (NBS; OMIM 251260), which is caused by *NBS1* mutations. Although NBS1 has been shown to bind to the T-cell receptor alpha (TCRα) locus, its role in TCRβ rearrangement is unclear. Hypomorphic mutations of *Nbs1* in mice and patients result in relatively mild T-cell deficiencies, raising the question of whether the truncated Nbs1 protein might have clouded a certain function of NBS1 in T-cell development. Here we show that the deletion of the entire Nbs1 protein in T-cell precursors (*Nbs1*$^{\text{T-del}}$) results in severe lymphopenia and a hindrance to the double-negative 3 (DN3)-to-DN4 transition in early T-cell development, due to abnormal TCRβ coding and signal joints as well as the functions of Nbs1 in T-cell expansion. Chromatin immunoprecipitation (ChIP) analysis of the TCR loci reveals that Nbs1 depletion compromises the loading of Mre11/Rad50 to V(D)J-generated DNA double-strand breaks (DSBs) and thereby affects resection of DNA termini and chromatin conformation of the postcleavage complex. Although a p53 deficiency relieves the DN3→DN4 transition block, neither a p53 deficiency nor ectopic expression of TCRαβ rescues the major T-cell loss in *Nbs1*$^{\text{T-del}}$ mice. All together, these results demonstrate that Nbs1's functions in both repair of V(D)J-generated DSBs and proliferation are essential for T-cell development.

DNA double-strand breaks (DSBs) are generated by exogenous DNA damage stimuli (e.g., ionizing radiation) and endogenous metabolic intermediates, such as collapsed replication forks. Upon DSB generation, NBS1 together with MRE11 and RAD50 form the MRN complex (26). MRE11, which contains two DNA binding domains, mediates the MRN complex binding to the exposed DNA ends. The adjacent MRN-associated DNA ends could be further tethered together through the coiled-coil domain (zinc hook) of RAD50 (19, 43). The chromatin loading of MRN stimulates the ATM kinase that subsequently phosphorylates the downstream effectors, such as p53 and CHK2, for cell cycle regulation, apoptosis, and repair initiation (9, 27, 40). In addition to transducing the repair signal, the NBS1/MRN complex participates in modulating DNA damage response (DDR) pathways by promoting error-free homology-directed repair (HDR) while repressing nonhomologous end joining (NHEJ) to minimize the generation of errant, therefore potentially "dangerous," DNA joints in S- and G_2/M-phase cells (47).

Mutations in any of the MRN complex proteins increase genomic instability and cause human genomic instability disorders. NBS1 hypomorphism causes the autosomal recessive disorder Nijmegen breakage syndrome (NBS; OMIM 251260). NBS patients show multisystemic defects, among which immunodeficiency and a predisposition to lymphoid malignancies originating from B- or T-cell lineages are the major hallmarks (11, 22). NBS patients are prone to opportunistic infections due to agammaglobulinemia, primarily IgA and IgG. Other immune defects include a reduced total number of $CD3^+$ and $CD4^+$ but not $CD8^+$ single-positive (SP) T cells (11, 22, 30). The MRN complex is therefore proposed to play an important role in the sensing (as a DDR component) and repairing (as a component of NHEJ) of V(D)J-generated DSBs and thereby to have its regulatory function in lymphoid development (2, 13). However, NBS patient cells carrying hypomorphic mutations of the *NBS1* gene fail to demonstrate a direct role of NBS1 in V(D)J recombination (15, 20, 48).

During lymphocyte development, G_1-phase-specific endonucleases RAG1/2 generate the DSBs at recombination signal sequences (RSS) flanking functional V, D, and J gene segments, which are in turn joined mainly by the NHEJ machinery (13, 28). Recent studies using intrachromosomal recombination substrates in the MRN hypomorphic mouse B cells or a small interfering RNA (siRNA) knockdown of MRN in cell lines demonstrate that the MRN complex stabilizes the DSB ends generated by RAG1/2 to promote canonical NHEJ (C-NHEJ; LigIV-Xrcc4 dependent) and also alternative NHEJ (A-NHEJ; LigIV-Xrcc4 independent) if C-NHEJ is not available (8, 10, 12, 17, 32, 34, 44, 46).

NBS1 consists of multiple domains and interacts with several key DDR molecules at both the early or late stages of the DDR cascade (49). While hypomorphic mutation supports cell and mouse survival, the complete loss of any of the MRN components causes embryonic lethality, suggesting a vital role of Nbs1

* Corresponding author. Mailing address: Leibniz Institute for Age Research-Fritz Lipmann Institute (FLI), Beutenbergstrasse 11, 07743 Jena, Germany. Phone: 49-3641-656415. Fax: 49-3641-656413. E-mail: zqwang@fli-leibniz.de.

# These authors contributed equally to the work.

† Supplemental material for this article may be found at http://mcb.asm.org/.

▽ Published ahead of print on 4 October 2010.

in viability and proliferation. Hypomorphic *Nbs1* mice show a T-lymphoid defect, characterized by a specific reduction of $CD4^+$ $CD8^+$ double-positive (DP) and $CD4^+$ single-positive (SP) T-cell populations but a rather normal amount of $CD8^+$ SP and $CD4^-$ $CD8^-$ double-negative (DN) T cells (17, 23). During T-cell development, Nbs1 localizes to the T-cell receptor alpha (TCRα) locus (7), and unjoined TCRα coding ends are accumulated in the hypomorphic *Nbs1* murine T cells (17). Collectively, these findings indicate that Nbs1/the MRN complex may function in V(D)J recombination during the late stage of T-cell development by specifically affecting the TCRα locus rearrangement (17). Given the essential function of NBS1, or MRN, in sensing and repairing DSBs, cell cycle control, and cell viability, full-length NBS1 may be expected to have a strong impact on lymphoid development. Current working models depicting that Nbs1 is involved in the repair of DSBs during V(D)J recombination have been developed from cells containing truncated Nbs1 isoforms (for example, p72), which may mask additional functions of NBS1. In the present study, we engineer mice with an Nbs1-specific deletion in early developing thymocytes and explore the additional function of the entire NBS1 protein in T-cell development, which might have not been seen previously in an *Nbs1* hypomorphic background.

MATERIALS AND METHODS

Generation of $Nbs1^{\text{T-del}}$, $Nbs1^{\text{T-del}}$ $p53^{-/-}$, and $Nbs1^{\text{F/F}}$ Lck-Cre$^+$ $Rag2^{-/-}$ AND^+ mice. $Nbs1^{\text{F6/F6}}$ mice (14) were crossed with Lck-Cre mice (kindly provided by Christopher Wilson, University of Washington, Seattle, WA), giving rise to $Nbs1^{\text{F6/F6}}$ Lck-Cre$^+$ mice, i.e., $Nbs1^{\text{T-del}}$ mice (mice with deletion of the entire Nbs1 protein in the T cells). Additionally, $Nbs1^{\text{T-del}}$ mice were crossed with *p53* knockout mice to generate $Nbs1^{\text{T-del}}$ $p53^{-/-}$ mice. In addition, $Nbs1^{\text{T-del}}$ mice were crossed with $Rag2^{+/-}$ AND^+ mice (kindly provided by André Nussenzweig, NIH) to generate mice with the genotype $Nbs1^{F6/F6}$ *Lck-Cre*$^+$ $Rag2^{-/-}$ AND^+ ($Nbs1^{\text{T-del}}$ $Rag2^{-/-}$ AND^+) (24, 36). All animals were maintained under specific-pathogen-free conditions at the animal facility of the Leibniz Institute for Age Research-Fritz Lipmann Institute (FLI), Jena, Germany. Animal care and experiments were performed in accordance with the ethic committee guidelines. For PCR genotyping, the following two primers were used to identify the $Nbs1^{\text{F6}}$ allele (1.2 kb) and the *Nbs1*-deleted (Δ) allele (0.6 kb): loxPtestR, AATACAG TGACTCCTGGAGG, and Intron5F, ATAAGACAGTCACCACTGCG. For a specific genotyping of the different stages of DN cells, the additional primer, EX6, CAGGGCGACATGAAAGAAAAC, together with the above-mentioned primers, was used to identify the $Nbs1^{\text{F6}}$ allele (0.3 kb) and the *Nbs1*-deleted (Δ) allele (0.6 kb). The *p53* knockout allele can be detected by PCR using the following primers: X7, TATACTCAGAGCCGGCCT; X6.5, ACAGCGTGGT GGTACCTTAT; and Neo, CATTCAGGACATAGCGTTGG. To genotype the *Rag2* knockout allele, we used 3f, GCAAGGACGCTCTAGGAATG, and 3r, TAGTCCCGTTTCCCATGTTG. To detect the TCRαβ transgene, the following primers were used: TCR-f, GACTTGGAGATTGCCAACCCATATCTA AGT, and TCR-r, TGAGCCGAAGGTGTAGTCGGAGTTTGCATT.

Flow cytometry analysis. The thymi and spleens were mashed through a 40-μm nylon membrane and then treated with the ACK buffer (0.15 mM NH_4Cl, 10 mM $KHCO_3$, 0.1 mM Na_2EDTA [pH 7.2]). The cells were resuspended in cold phosphate-buffered saline (PBS) containing 2% fetal calf serum (FCS), subjected to staining with phycoerythrin (PE)-, fluorescein isothiocyanate (FITC)-, allophycocyanin (APC)-, and PE-Cy5-conjugated monoclonal antibodies, and analyzed with a FACSCanto flow cytometer equipped with FACSDiva software (Becton Dickinson, Mountain View, CA). The panel of FITC-labeled monoclonal antibodies included CD19 and CD44 (Pharmingen, San Diego, CA). The PE-conjugated antibodies used were CD25, CD3, and CD4 (Pharmingen). The APC and PE-Cy5-conjugated antibodies used were CD8 and CD4 (Pharmingen). Apoptosis was analyzed by staining cells with FITC-conjugated annexin V antibody (Pharmingen) in the annexin V staining solution (10 mM HEPES-NaOH at pH 7.4, 140 mM NaCl, 2.5 mM $CaCl_2$).

Lymphocyte sorting and stimulation. After the T-cell isolation and antibody staining, the DN, DP, and SP thymocyte subpopulations were purified from thymi to >95% purity using a FACSAria cell sorter (Becton Dickinson). For *in vitro* T-cell stimulation, sorted thymocytes were treated simultaneously with anti-CD3 and anti-CD28 antibodies (10 μg/ml each) or 5 μg/ml phytohemagglutinin (PHA; Sigma-Aldrich, Munich, Germany) together with 10 ng/ml phorbol myristate acetate (PMA; Sigma-Aldrich). Prior to stimulation, lymphocytes were stained with 2.5 μM carboxyfluorescein diacetate succinimidyl ester (CFSE) (29). The cells were analyzed by flow cytometry at the indicated time.

V(D)J recombination profiling. Genomic DNA was isolated from the sorted DP, SP, and DN T cells and amplified by PCR using the following primers: for the β locus coding joint, Vβ13, 5′-GAGGAAAGGTGACATTGAGC-3′, and Jβ2.7, 5′-TGAGAGCTGTCTCCTACTATCGATT-3′; for the β locus signal joint (5), Dβ1, 5′-AGAGGAGCAGCTTATCTGGTGG-3′, and Vβ14, 5′-CTT TGGTGACTTCTGACTTGA-3′; and for the α locus signal joint (38), SJα56, 5′-CAGTAGGGGATGGATGCTAACATGA-3′, and ADV8-RS, 5′-CCTGCA CCCTTGGTTCATGTG-3′.

The PCR products were gel purified and subsequently cloned into the PCR-Topo TA vector (Invitrogen, Karlsruhe, Germany). The sequences were compared with those in the UCSC database (http://genome.ucsc.edu/) for a further characterization of the resolved V(D)J recombination. The raw sequences of the TCR status are provided in Tables S1 to S4 in the supplemental material.

ChIP assay. Freshly isolated thymocytes (1×10^7) were cross-linked with 1% formaldehyde, and chromatin immunoprecipitations (ChIPs) were performed as described previously (18) using 4 μg of a polyclonal antibody specific for Rad50 (Upstate, Lake Placid, NY), γ-H2AX (Upstate), or acetyl-histone H4 (Ac-H4; Upstate). Input DNA and immunoprecipitated DNA were analyzed by PCR for the presence of Vβ1, Vβ30, Vα5, and Vα21 recombination signal sequences (RSSs). The primers used to amplify the sequences of interest included the following: Vβ1, 5′CTGGGGACAAAGAGGTCAAA3′ and 5′GGGAAGTCTG GGTAGGAAGG3′; Vβ30, 5′TCTGGGGCTACAGCTGATTT3′ and 5′GCAT TAGGCATGAGGGAAAA3′; Vα5, 5′CTGGGAAGCGTCTTCAGTTC3′ and 5′AAAAGTGTGCCACTCCATCC3′; and Vα21, 5′TTGGTACCGACAGGTT CCTC3′ and 5′TGCTGAGCTCATTGCTCACT3′. PCR products were resolved on a 2% agarose gel and stained with ethidium bromide.

Chromosome metaphase preparation and cytogenetic analysis. The thymocytes from 8-week-old control and $Nbs1^{\text{T-del}}$ mice were isolated as described above. Thymocytes (1×10^7 to 5×10^7) were cultured in complete RPMI 1640 medium supplemented with 10% FCS and stimulated with 10 units/ml interleukin-2 (IL-2; Chiron, Ratingen, Germany), 10 ng/ml PMA (Sigma-Aldrich), and 750 ng/ml ionomycin (Sigma-Aldrich) (33). After 48 h of incubation at 37°C, 20 ng/ml colcemid (Sigma-Aldrich) was added, and the metaphases were prepared according to the standard protocol. For telomere fluorescence *in situ* hybridization (T-FISH), hybridization of FITC-labeled peptide nucleic acid (PNA) telomeric probes (Dako, Hamburg, Germany) onto metaphases was conducted by following the company's manual. The pictures of metaphase were captured and analyzed by BandView and FISHView softwares (Applied Spectral Imaging system) installed on a Zeiss Imager M1 microscope.

Immunoblotting. Proteins extracted from cells in a RIPA buffer (20 mM HEPES at pH 7.6, 20% glycerol, 0.5 M NaCl, 1.5 mM $MgCl_2$, 0.2 mM EDTA at pH 8.0, 0.5% NP-40, 1 mM dithiothreitol [DTT], 1 mM phenylmethylsulfonyl fluoride [PMSF], 5 mg/ml leupeptin, 2 mg/ml aprotinin, 1 mM β-glycerophosphate, 1 mM Na_3VO_4, and 10 mM NaF) were resolved by sodium dodecyl sulfate-polyacrylamide gel electrophoresis (SDS-PAGE), blotted with antibodies in 1× Tris-buffered saline–Tween 20 (TBS-T) containing 5% nonfat dried milk, followed by an incubation with horseradish peroxidase-conjugated secondary antibodies, and detected by ECL reagents (Amersham Biosciences, Buckinghamshire, United Kingdom). The following antibodies were used: rabbit anti-Nbs1 antibody (1:1,000; Cell Signaling, Danvers, MA), mouse anti-PARP-1 (1:2,000; R&D Systems, Wiesbaden-Nordenstadt, Germany), and mouse anti-Chk2 (1:1,000; Upstate).

Histopathology and immunohistological staining. The tissues used for histological examination were fixed in 4% buffered formalin and embedded in paraffin. The sections (5 μm) were stained with hematoxylin and eosin (H&E) and mounted for microscopy. The pictures are processed with AxioVision software.

RESULTS

T-cell-specific deletion of *Nbs1* in mice results in central and peripheral T-cell lymphopenia. To investigate the essential function of Nbs1 in lymphoid development and V(D)J recombination, we crossed $Nbs1^{\text{F6/F6}}$ mice (14) with Lck-Cre transgenic mice, which express Cre recombinase in T-cell precursors

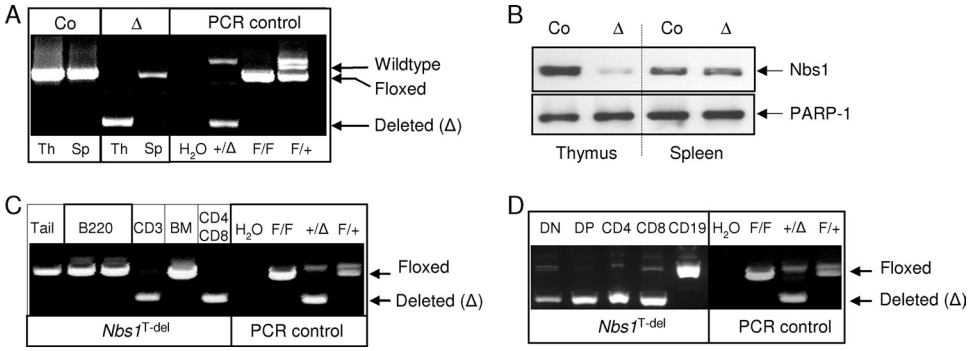

FIG. 1. The specific deletion of *Nbs1* in the T-cell lineage. (A) PCR analysis of the *Nbs1* deletion in the thymus (Th) and spleen (Sp) of the indicated genotype. "Co" and "Δ" represent samples obtained from $Nbs1^{\text{T-ctr}}$ and $Nbs1^{\text{T-del}}$ mice, respectively. PCR controls used $Nbs1^{\text{F6}}$ (F) and *Nbs1*-deleted (Δ) alleles. (B) Western blot analysis of the Nbs1 deletion in thymi and spleens of 4-week-old $Nbs1^{\text{T-ctr}}$ and $Nbs1^{\text{T-del}}$ mice. PARP-1 is used as a loading control. (C) PCR analysis of the *Nbs1* deletion in genomic DNA from sorted $CD3^+$, $B220^+$, and $CD4^+$ $CD8^+$ populations from $Nbs1^{\text{T-del}}$ thymi and spleens as well as bone marrow (BM) cells. Tail DNA (tail) is used to control the floxed allele. (D) PCR analysis of the *Nbs1* deletion in sorted $CD19^+$, $CD4^+$, $CD8^+$, and $CD4^+$ $CD8^+$ populations from $Nbs1^{\text{T-del}}$ thymi and spleens.

(DN cells). PCR and Western blot analyses confirmed that $Nbs1^{\text{F6/F6}}$ Lck-Cre^+ mice had a deletion of *Nbs1* specifically in the thymi and all T-cell populations but not $CD19^+$ B cells (Fig. 1A to D). Hence, we designated $Nbs1^{\text{F6/F6}}$ Lck-Cre^+ as $Nbs1^{\text{T-del}}$. The control group of mice ($Nbs1^{\text{T-ctr}}$) includes $Nbs1^{+/+}$ Lck-Cre^-, $Nbs1^{+/+}$ Lck-Cre^+, $Nbs1^{+/\text{F6}}$ Lck-Cre^-, $Nbs1^{+/\text{F6}}$ Lck-Cre^+, and $Nbs1^{\text{F6/F6}}$ Lck-Cre^- mice, all of which carried at least one functional *Nbs1* allele.

Young $Nbs1^{\text{T-del}}$ mice exhibited a marked atrophy of the medullar compartment in the thymi (Fig. 2A). Flow cytometry analysis of the thymi and spleens from 4-week-old mice revealed a greatly reduced cellularity and proportion of all distinct T-cell populations. Whereas the average cellularity of DP cells was 10×10^7 in $Nbs1^{\text{T-ctr}}$ mice, it reached only 4.6×10^7 in $Nbs1^{\text{T-del}}$ mice (~2-fold reduction) (Fig. 2B). The reduction of $CD4^+$ or $CD8^+$ SP thymocytes was even more pronounced, from 1.1×10^7 $CD4^+$ SP cells in $Nbs1^{\text{T-ctr}}$ mice to 0.17×10^7 $CD4^+$ SP cells in $Nbs1^{\text{T-del}}$ mice (~6.5-fold reduction) and from 0.26×10^7 $CD8^+$ SP cells in $Nbs1^{\text{T-ctr}}$ to 0.03×10^7 $CD8^+$ SP cells in $Nbs1^{\text{T-del}}$ mice (~8.7-fold reduction) (Fig. 2C). The relative frequency and cellularity of $CD4^+$ and $CD8^+$ SP cells were also reduced in the $Nbs1^{\text{T-del}}$ spleen and blood samples (Fig. 2C and D; also data not shown). Among the general loss of SP cells, TCRα2- and TCRα8.3-expressing mature T cells were greatly reduced (data not shown). In addition, a considerably high percentage of apoptotic T cells was present in the thymi and spleens from mutants (Fig. 2E). After *in vitro* stimulation with PHA/PMA or TCR cross-linking antibodies (against CD3/CD28), $Nbs1^{\text{T-del}}$ T cells failed to proliferate (Fig. 3A and C) and showed prominent apoptosis (Fig. 3B and D), which is similar to the response of NBS patient T cells (42). All these data demonstrate dramatic defects of T-cell development and function when *Nbs1* is completely deleted in an early stage.

Since ATM and NBS1 act in the same pathway upon DSB generation (27), we further compared the T-cell profile of $Atm^{-/-}$ mice with that of our $Nbs1^{\text{T-del}}$ mice (1). $Atm^{-/-}$ mice showed only a mild percentage of $CD4^+$ SP reduction but no reduction of $CD8^+$ SP cells compared to those of wild-type controls (Fig. 2F), which is consistent with previous reports (1, 41). Compared to $Atm^{-/-}$ mice, $Nbs1^{\text{T-del}}$ mice have significantly fewer $CD4^+$ and $CD8^+$ SP cells in the thymi and also in the spleens (Fig. 2F). These data seem to indicate that the functions of ATM and NBS1 in T-cell development are not identical, despite their biochemical functions in the same DSB response.

The absence of Nbs1 specifically hampers the DN3-to-DN4 transition in T-cell development. To determine the stage at which T-lymphocyte development is affected, we investigated early T-cell development from T-cell precursors. Double staining with CD25 and CD44 antibodies, which mark the developmental stages before TCRα rearrangement, revealed that the $Nbs1^{\text{T-del}}$ thymus contained normal or even slightly higher double-negative 1 (DN1; $CD44^+$ $CD25^-$), DN2 ($CD44^+$ $CD25^+$), and DN3 ($CD44^-$ $CD25^+$) populations (Fig. 4A). However, the frequency of $Nbs1^{\text{T-del}}$ DN4 ($CD44^-$ $CD25^-$) cells was significantly decreased (21.2%) compared to that of controls (34.5%; $P = 0.029$) (Fig. 4A). PCR analysis revealed that the *Nbs1* deletion was readily detectable at the DN1 stage, and the majority (>80%) was deleted at the DN3 stage (Fig. 4B). It seems that the percentage of DN4 cells (Fig. 4A) in our $Nbs1^{\text{T-del}}$ mice was overrepresented because a high fraction of DN4 cells (~50%) still contained the intact *Nbs1* allele (Fig. 4B), which might be derived from DN3 cells escaping the deletion of the *Nbs1* locus.

Loss of Nbs1 impairs the processing of V(D)J-associated DSBs in TCRβ coding joints. The transition from DN3 to DN4 corresponds to the stage of TCRβ gene rearrangement (16). To further investigate how Nbs1 contributes to the repair of DSBs in V(D)J recombination, we analyzed the V(D)J coding joints of the TCRβ locus in $Nbs1^{\text{T-del}}$ T cells. To this end, we chose and amplified Vβ13-Dβ1/2-Jβ2.7 recombination products by PCR and sequenced these joints (Fig. 5A; see also Tables S1 and S2 in the supplemental material). We found that $Nbs1^{\text{T-del}}$ T cells had a significantly higher portion of V(D)J joints with longer Dβ segments (93% in mutants compared to 73% in controls; here, we used 4 nucleotides [nt] as the threshold to define long or short Dβ1/2 segments) (Fig. 5B and C; see also Tables S1 and S2 in the supplemental material). Meanwhile, the nucleotide insertion rate in the Vβ13-Dβ1/2 junc-

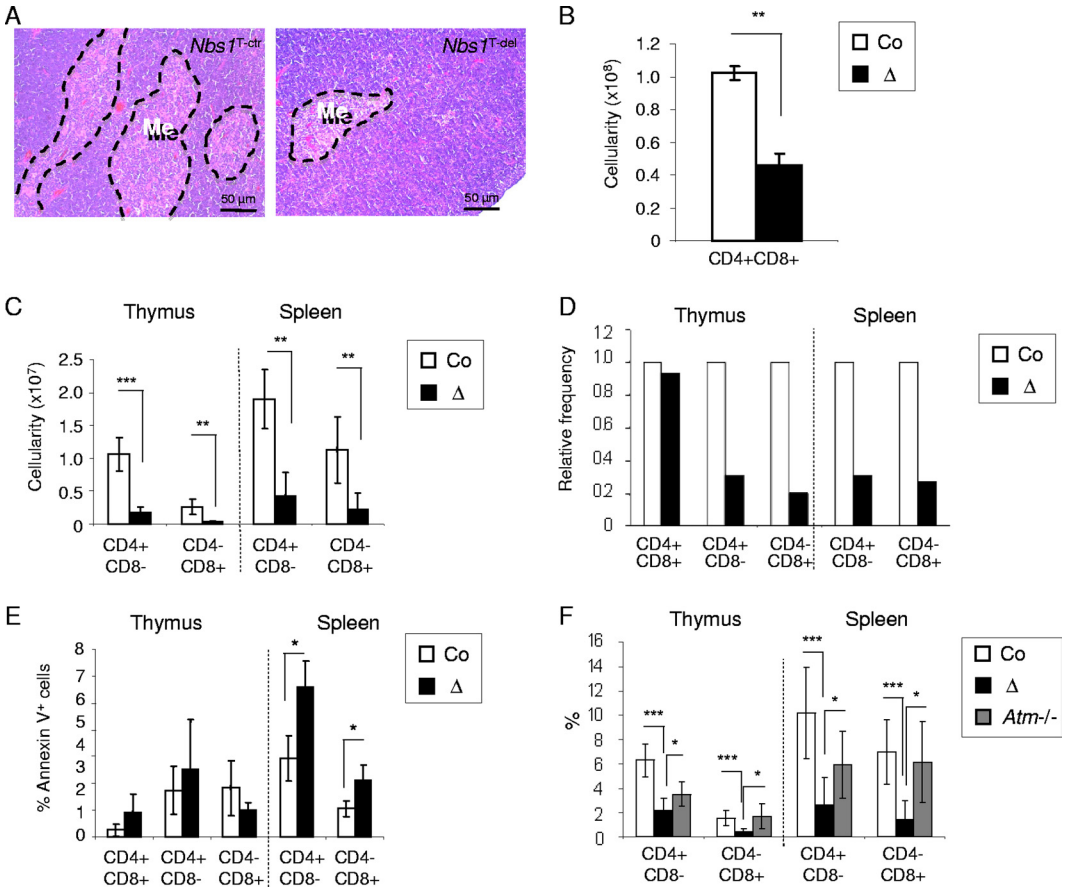

FIG. 2. *Nbs1*$^{T\text{-}del}$ mice develop central and peripheral T-cell lymphopenia. (A) H&E staining of thymus sections from 4-week-old *Nbs1*$^{T\text{-}ctr}$ and *Nbs1*$^{T\text{-}del}$ mice. Me, medulla. (B) Numbers of CD4$^+$ CD8$^+$ DP T cells in the thymi of *Nbs1*$^{T\text{-}ctr}$ and *Nbs1*$^{T\text{-}del}$ mice ($n > 6$; 3 to 5 weeks of age). (C) Numbers of CD4$^+$ and CD8$^+$ SP T cells in the thymi and spleens of *Nbs1*$^{T\text{-}del}$ mice are compared to those in the thymi and spleens of *Nbs1*$^{T\text{-}ctr}$ mice ($n > 6$; 3 to 5 weeks of age). (D) Frequency of CD4$^+$ CD8$^+$ DP, CD4$^+$ SP, and CD8$^+$ SP T cells in the thymi and spleens of *Nbs1*$^{T\text{-}del}$ mice relative to the controls ($n > 6$; 3 to 5 weeks of age). (E) Proportion of annexin V-positive T cells in the thymi and spleens of *Nbs1*$^{T\text{-}ctr}$ and *Nbs1*$^{T\text{-}del}$ mice. (F) Comparison of lymphopenia in *Nbs1*$^{T\text{-}del}$ and *Atm*$^{-/-}$ mice. The histogram shows the comparison of the average percentages of CD4$^+$ and CD8$^+$ SP T cells in the thymi and spleens of *Nbs1*$^{T\text{-}ctr}$, *Nbs1*$^{T\text{-}del}$, and *Atm*$^{-/-}$ mice ($n > 4$; 3 to 5 weeks of age). Co, *Nbs1*$^{T\text{-}ctr}$; Δ, *Nbs1*$^{T\text{-}del}$; *, $P < 0.05$; **, $P < 0.01$; ***, $P < 0.001$. P values were obtained using Student's unpaired t test.

tion region was also significantly increased (63% in controls versus 84% in mutants; $P < 0.05$) (Fig. 5B and C) and similarly increased in the Dβ1/2-Jβ2.7 joint, where the nucleotide insertion rate was consistently elevated albeit not statistically significant (66% in controls versus 77% in mutants; $P > 0.05$). In addition, for the Vβ13-Dβ1/2-Jβ2.7 coding joint deletion, we detected less frequently degraded coding ends during V(D)J recombination, although they cannot reach a statistically significant level ($P > 0.05$) (Fig. 5B and C). Nevertheless, as combined consequences of the above-mentioned phenotypes, the *Nbs1*$^{T\text{-}del}$ T cells had formed longer coding joint regions than those of controls (6.2 nt in *Nbs1*$^{T\text{-}del}$ versus 3.5 nt in controls; $P < 0.05$) (Fig. 5D). These findings suggest a defective DNA end processing or a resection of V(D)J termini when *Nbs1* is completely deleted.

Nbs1 deletion affects the joining of signal joints. To test if a complete Nbs1 loss also affects signal joint formation, we examined signal joints for Vβ14-Dβ1 and Jα56-ADV8 (5, 38). A sequence analysis of cloned PCR products showed that more than 55% of the signal regions in both control and *Nbs1*$^{T\text{-}del}$ T cells had perfect joining (see Tables S3 and S4 in the supplemental material), indicating that *Nbs1*$^{T\text{-}del}$ mice have robust signal joint formation. This is consistent with the previous report which found that c-Abl-transformed MRN hypomorphic B cells have normal signal joint formation (10, 17). However, in those signal joints with imperfect joining, *Nbs1*-null T cells showed a high preference for the usages of the GC nucleotide rather than those of the AT nucleotide. For the β locus, the GC/AT ratio is 1.03 in *Nbs1*$^{T\text{-}ctr}$ T cells and 3.86 in *Nbs1*$^{T\text{-}del}$ T cells ($P < 0.01$); for the α locus, the GC/AT ratio is 1.5 in *Nbs1*$^{T\text{-}ctr}$ T cells and 2.1 in *Nbs1*$^{T\text{-}del}$ T cells ($P > 0.05$) (Fig. 5E; see also Tables S3 and S4 in the supplemental material). These interesting results suggest altered terminal deoxynucleotidyltransferase (TdT) activity in the TCRαβ loci in the absence of *Nbs1*.

Rag-induced DSB repair and chromatin conformation around V(D)J segments in *Nbs1*$^{T\text{-}del}$ T cells. MRN helps stabilize the coding joints in the "postcleavage complex," and the enzymatic activity of Mre11 can process DSB ends (10, 44). The abnormalities in V(D)J joints, especially in TCRβ coding

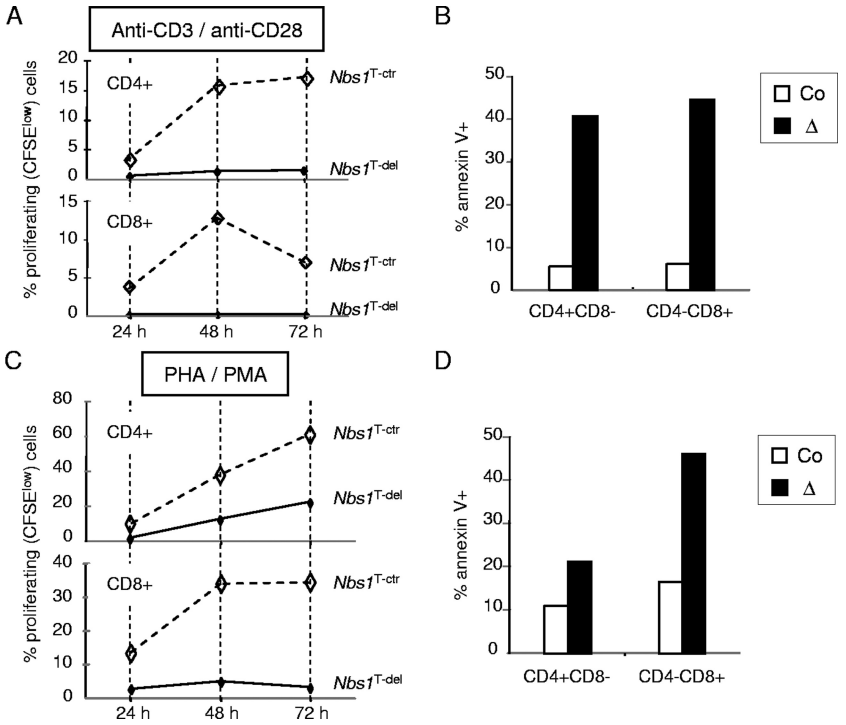

FIG. 3. Cellular response to T-cell activation in *Nbs1*$^{\text{T-del}}$ mice. (A) Thymocytes were stimulated with anti-CD3/anti-CD28 antibodies and labeled with CFSE. The proliferation of *Nbs1*$^{\text{T-ctr}}$ and *Nbs1*$^{\text{T-del}}$ CD4$^+$ and CD8$^+$ SP T cells was analyzed at the indicated time points by flow cytometry, according to the CFSE dilution. (B) Apoptotic cells after stimulation with anti-CD3/anti-CD28 antibodies were determined by annexin V staining. (C) Thymocytes were stimulated with PMA/PHA and labeled with CFSE. The proliferation of *Nbs1*$^{\text{T-ctr}}$ and *Nbs1*$^{\text{T-del}}$ CD4$^+$ and CD8$^+$ SP T cells was analyzed at the indicated time points by flow cytometry, according to the CFSE dilution. (D) Apoptosis after PMA/PHA treatment was determined by annexin V staining. Co, *Nbs1*$^{\text{T-ctr}}$; Δ, *Nbs1*$^{\text{T-del}}$.

joints of *Nbs1*$^{\text{T-del}}$ T cells, may reflect the *Nbs1*-null-mediated DSB repair defect to process coding ends prior to joining. To gain insight into the impact of the *Nbs1*-null mutation in V(D)J end processing and stability, we analyzed the DSB repair status around Rag-induced DSB sites by chromatin immunoprecipitation (ChIP) (Fig. 6A). We first examined the status of γ-H2AX, a DSB marker, in the V(D)J joints in both distal and proximal V regions of TCRβ and -α loci (Vβ1, Vβ30, Vα5, and

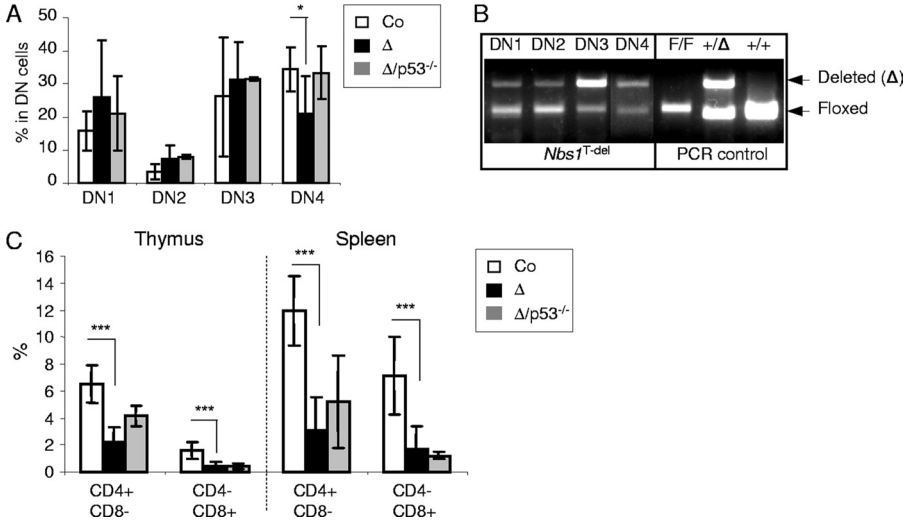

FIG. 4. The *Nbs1*-null mutation affects the transition from the DN3 to DN4 stages in early T-cell development. (A) The histogram shows the different DN subpopulations in the total DN population, according to their surface markers CD44 and CD25. These data are the mean percentages for at least 6 mice from each genotype. (B) PCR analysis of the *Nbs1* deletion in sorted DN subpopulations, according to their CD44 and CD25 expression profiles. F, *Nbs1* floxed allele; Δ, *Nbs1*-deleted allele. (C) Frequencies of CD4$^+$ and CD8$^+$ SP T cells obtained from 4-week-old littermates of *Nbs1*$^{\text{T-ctr}}$, *Nbs1*$^{\text{T-del}}$, and *Nbs1*$^{\text{T-del}}$ *p53*$^{-/-}$ mice. These data are the mean percentages for at least three mice from each genotype. Co, *Nbs1*$^{\text{T-ctr}}$; Δ, *Nbs1*$^{\text{T-del}}$; Δ/p53, *Nbs1*$^{\text{T-del}}$ *p53*$^{-/-}$; ⋆, $P < 0.05$; ⋆⋆⋆, $P < 0.001$. *P* values were obtained using Student's unpaired *t* test.

A

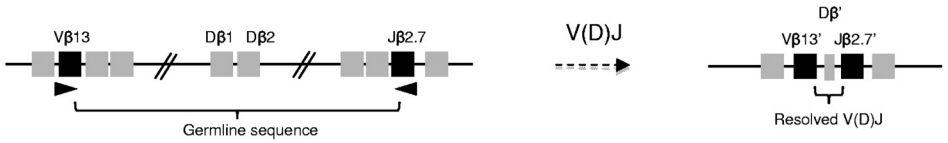

B

β locus Junction characteristics		*Nbs1*$^{T\text{-}ctr}$ (n = 41)		*Nbs1*$^{T\text{-}del}$ (n = 31)	
		size	Frequency (%)	size	Frequency (%)
Deletion	Vβ13 segment	-2.32	30/41 (73)	-2.36	21/31 (68)
	Dβ1/2 ≤ 4nt	6.98	11/41 (27)	7.61	2/31 (7)**
	Jβ2.7 segment	-3.93	35/41 (85)	-3.29	23/31 (74)
Insertion	P/N addition in VD	+1.59	26/41 (63)	+2.10	26/31 (84)*
	P/N addition in DJ	+1.34	27/41 (66)	+2.10	24/31 (77)

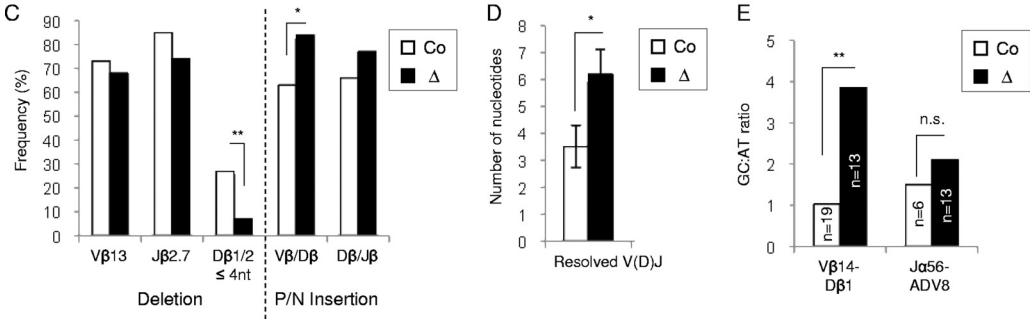

FIG. 5. *Nbs1* deletion results in aberrant processing of V(D)J coding ends and signal ends. (A) Scheme for V(D)J recombination in TCR Vβ 13, Dβ1 or Dβ2, and Jβ 2.7 gene loci. Arrowheads indicate primer positions. (B) TCRβ gene rearrangement analyzed by sequencing the PCR products of indicated segments in genomic DNA isolated from 4-week-old *Nbs1*$^{T\text{-}ctr}$ and *Nbs1*$^{T\text{-}del}$ thymocytes. *n*, number of PCR products analyzed. The original data are shown in Tables S1 and S2 in the supplemental material. (C) PCR sequencing analysis of TCRβ gene rearrangements in thymocyte DNA isolated from 4-week-old *Nbs1*$^{T\text{-}ctr}$ and *Nbs1*$^{T\text{-}del}$ mice. The frequency of the V(D)J joints is plotted. (D) Size of resolved Vβ13-Dβ1/2-Jβ2.7 regions in *Nbs1*$^{T\text{-}ctr}$ and *Nbs1*$^{T\text{-}del}$ mice. (E) Nucleotide usages in Vβ14-Dβ1 and Jα56-ADV8 signal joints of control and *Nbs1*$^{T\text{-}del}$ mice (*n*, number of sequences used for the GC/AT ratio calculation). The *P* value is calculated using the percentage of GC in imperfect joints (see Tables S3 and S4 in the supplemental material). Co, *Nbs1*$^{T\text{-}ctr}$; Δ, *Nbs1*$^{T\text{-}del}$; *, $P < 0.05$; **, $P < 0.01$; n.s., not significant. The chi-square test was used for calculations in panels B and C, and the unpaired Student's *t* test was used for calculations in panels D and E.

Vα21). We recovered more γ-H2AX products from these regions in the *Nbs1*-null T cells than in controls, suggesting that Rag1/2-induced DSBs were persistent, reflecting inefficient repair in *Nbs1*-null T cells (Fig. 6A). Consistent with this notion, using the RAD50 antibody, we precipitated fewer products from *Nbs1*$^{T\text{-}del}$ T-cell extracts than from control cell extracts (Fig. 6A). This indicates that Rad50 loading to DSBs was compromised because of the *Nbs1* deletion, which in turn might impair the stability and thereby the processing of the DSB ends. Since the H2AX phosphorylation-mediated chromatin response to DSBs facilitates MRN loading and further DNA end processing (37), we next monitored the chromatin status around V(D)J ends using an antibody against acetylhistone H4 (Ac-H4), a marker of a relaxed chromatin conformation. Consistent with the γ-H2AX status, we found more products from V segments in *Nbs1*$^{T\text{-}del}$ thymocytes than from those in controls, indicating an open chromatin conformation around these gene segments (Fig. 6A). All together, the initiation of the DSB response in *Nbs1*$^{T\text{-}del}$ T cells seems normal, as indicated by the presence of γ-H2AX, but the processing of V(D)J termini is compromised.

The persistence of the γ-H2AX and relaxed chromatin in *Nbs1*$^{T\text{-}del}$ T cells indicates the defects in the repair process without Nbs1. We further confirmed the DNA repair defect in the *Nbs1*-null T cells by cytogenetic analysis of thymocytes upon treatment with PMA/IL-2/ionomycin. While the chromosome numbers were unchanged in *Nbs1*$^{T\text{-}del}$ T cells, we found significantly higher frequencies of chromosomal breaks and fusions in *Nbs1*$^{T\text{-}del}$ T cells than in *Nbs1*$^{T\text{-}ctr}$ T cells (Fig. 6B). In total, 73% of *Nbs1*$^{T\text{-}del}$ metaphases contained at least one aberration, in contrast to 53% in the control group ($P < 0.01$) (Fig. 6B). The defect is most likely mediated by the ATM-CHK2 pathway rather than the ATR-CHK1 pathway, since *Nbs1*$^{T\text{-}del}$ T cells show an attenuated ATM-CHK2 pathway (Fig. 6C) but not an attenuated ATR-CHK1 pathway (data not shown) after an *in vitro* challenge of *Nbs1*$^{T\text{-}del}$ T cells with adriamycin and UV, which is consistent with previous observations (35).

A p53 deficiency and the TCR transgene cannot fully correct *Nbs1*$^{T\text{-}del}$ lymphopenia. T-cell lymphopenia in *Nbs1*$^{T\text{-}del}$ mice could be a combined defect of a Nbs1-mediated repair of DSBs and of proliferation. The transition from DN3 to DN4 corresponds to the stage of TCRβ gene rearrangement (16), and the reduction of DN4 cells in *Nbs1*$^{T\text{-}del}$ mice implies a defective *Nbs1* function in repairing V(D)J-associated DSBs in the TCRβ locus, which could trigger the p53-dependent apoptotic

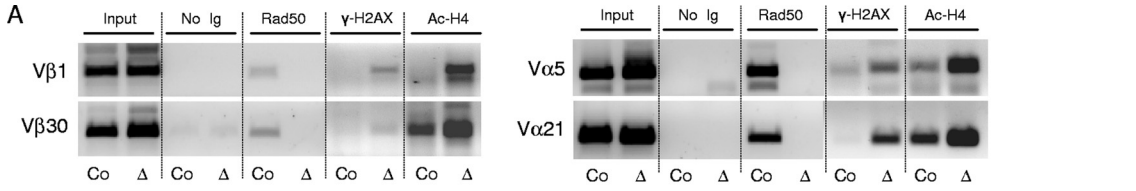

Genotype	Chromosome No. per metaphase	Total chromosome breaks (frequency)	Chromosome fusions (frequency)	% Aberration / metaphases
Nbs1$^{T\text{-}ctr}$	39.53 ± 2.26 (n = 77)	52 / 77 (0.68) 24 chromatid breaks 28 chromosome breaks	2 (n = 34; 6%)	53%
Nbs1$^{T\text{-}del}$	39.35 ± 1.82 (n = 75)	117 / 75 (1.56)** 75 chromatid breaks 42 chromosome	8 (n = 35; 23%)	73%**

FIG. 6. Defects in V(D)J-initiated DNA repair, chromosome instability, and impaired DDR in Nbs1-deleted T cells. (A) ChIP analysis using antibodies against Rad50, γ-H2AX, and Ac-H4. These antibodies recovered distal and proximal Vβ (left) and Vα (right) regions of *Nbs1*$^{T\text{-}ctr}$ and *Nbs1*$^{T\text{-}del}$ thymocytes. Co, *Nbs1*$^{T\text{-}ctr}$; Δ, *Nbs1*$^{T\text{-}del}$; γ-H2AX, phospho-histone H2AX; Ac-H4, acetyl-histone H4. (B) Summary of the chromosomal stability in *Nbs1*$^{T\text{-}ctr}$ and *Nbs1*$^{T\text{-}del}$ T cells. The metaphases were prepared from 8-week-old *Nbs1*$^{T\text{-}ctr}$ and *Nbs1*$^{T\text{-}del}$ T cells 48 h after IL-2/PMA/ionomycin stimulation. *n*, number of metaphases analyzed. **, $P < 0.01$. Student's unpaired *t* test was used, except that the chi-square test was applied for calculation of the percentage of metaphases containing aberrations. (C) Western blot analysis of Nbs1 and Chk2 in whole-cell extracts from *Nbs1*$^{T\text{-}ctr}$ and *Nbs1*$^{T\text{-}del}$ thymocytes after 2 h of treatment with 0.2 μg/ml of adriamycin (Adr). PARP-1 is used as a loading control. The ratio of the phosphorylated form of Chk2 (upper band) was corrected to that of the nonphosphorylated form (lower band) by ImageJ software and indicated under the corresponding lanes. NA, not applicable.

pathway. In order to test this hypothesis, we crossed *Nbs1*$^{T\text{-}del}$ mice into a p53-deficient background. A p53 deletion in *Nbs1*$^{T\text{-}del}$ mice completely restored the DN4 cell population (Fig. 4A), suggesting that the affected DN3-to-DN4 transition was likely DNA breaks based and mediated by p53 activation. Although a p53 deficiency could rescue the DN4 cell loss in *Nbs1*$^{T\text{-}del}$ mice, the survival advantage given by the p53 loss did not significantly increase the total number of immature DP and mature SP T cells in the *Nbs1*$^{T\text{-}del}$ thymus and spleen (Fig. 4C). It is possible that the T-cell lymphopenia in *Nbs1*$^{T\text{-}del}$ mice is caused by the failure of resolving the V(D)J recombination termini and by the subsequent membrane-bound death receptor-mediated positive and negative selection or proliferation defects.

To further examine the contribution of DSBs and TCR function-mediated T-cell loss in the absence of Nbs1, we crossed *Nbs1*$^{T\text{-}del}$ mice into the *Rag2*$^{-/-}$ *AND*$^{+}$ genetic background. *Rag2*$^{-/-}$ *AND*$^{+}$ mice are devoid of endogenous V(D)J recombination because they lack Rag2-mediated DSBs in TCRs, but they ectopically express the transgenic TCRαβ receptor (AND^{+}) (24, 36). *Nbs1*$^{T\text{-}del}$ *Rag2*$^{-/-}$ *AND*$^{+}$ mice reached 26% of the thymic cellularity of *Nbs1*$^{T\text{-}ctr}$ *Rag2*$^{-/-}$ *AND*$^{+}$ controls (Fig. 7A). In addition, the CD4^{+} SP fraction in *Nbs1*$^{T\text{-}del}$ *Rag2*$^{-/-}$ *AND*$^{+}$ mice was about 51% of that of the *Nbs1*$^{T\text{-}ctr}$ *Rag2*$^{-/-}$ *AND*$^{+}$ controls (29% in *Nbs1*$^{T\text{-}del}$ *Rag2*$^{-/-}$ *AND*$^{+}$ mice and 57% in *Nbs1*$^{T\text{-}ctr}$ *Rag2*$^{-/-}$ *AND*$^{+}$ mice) (Fig. 7B). Under the condition of *Rag2* deficiency, the TCRαβ transgene partially restored the mature CD4^{+} T cells in the *Nbs1*$^{T\text{-}del}$ mice (51%, in comparison with ~30% left in the *Rag2*$^{+/+}$ background) (Fig. 2B and 7B). Despite this increased frequency, the total number of CD4^{+} SP cells was still significantly lower in *Nbs1*$^{T\text{-}del}$ *Rag2*$^{-/-}$ *AND*$^{+}$ mice than in controls (Fig. 7C), arguing for a role of Nbs1 in T-cell proliferation and viability.

DISCUSSION

A complete deletion of Nbs1 in the T-cell lineage resulted in a >6-fold reduction of CD4^{+} and CD8^{+} SP T cells and a 2-fold reduction of DP cells. These findings are in contrast with an approximately 2- to 3-fold reduction of CD4^{+} SP cells and yet a normal level of CD8^{+} SP cells in human NBS patients for whom NBS1 is hypomorphic (11, 22, 30). Moreover, hypomorphic mutations of *Nbs1* in mice resulted in about a 30% reduction of SP T cells and DP T cells (17, 23). The mild T-cell phenotype of hypomorphic NBS1 in humans and mice is likely attributable to the presence of a truncated NBS1 protein, which supports survival and possibly proliferation (see below). Notably, although ATM and NBS1 act in a common DDR pathway *in vitro*, compared to our *Nbs1*$^{T\text{-}del}$ mice, *Atm*-null thymi show roughly a 25% reduction of the total cellularity but a normal frequency of CD4^{+} CD8^{+} DP cells and CD8^{+} SP cells (1, 41) (Fig. 2F).

V(D)J analysis of hypomorphic mutant *Nbs1* and *Mre11* mice and *Atm*-null mice reveals very similar V(D)J recombination defects, particularly in the TCRα locus, marked by unrepaired coding ends (17, 41). It seems that hypomorphic Nbs1 or Mre11 proteins and full-length Atm play largely overlapping roles in V(D)J processing and rather affect the later stage of T-cell development. In our study, in addition to recapitulating the later defect of TCRα locus recombination, as shown in *Atm*$^{-/-}$ mice and *Nbs1*/*Mre11* hypomorphic mice (17, 21), the deletion of the complete *Nbs1* protein in T cells unexpectedly affects the T-cell development as early as in the DN3-to-DN4 transition, which has not been reported in hypomophic MRN mutant mice or *Atm*-null mice. The similar but discrepant T-cell phenotypes of *Atm*-null and T-cell-specific

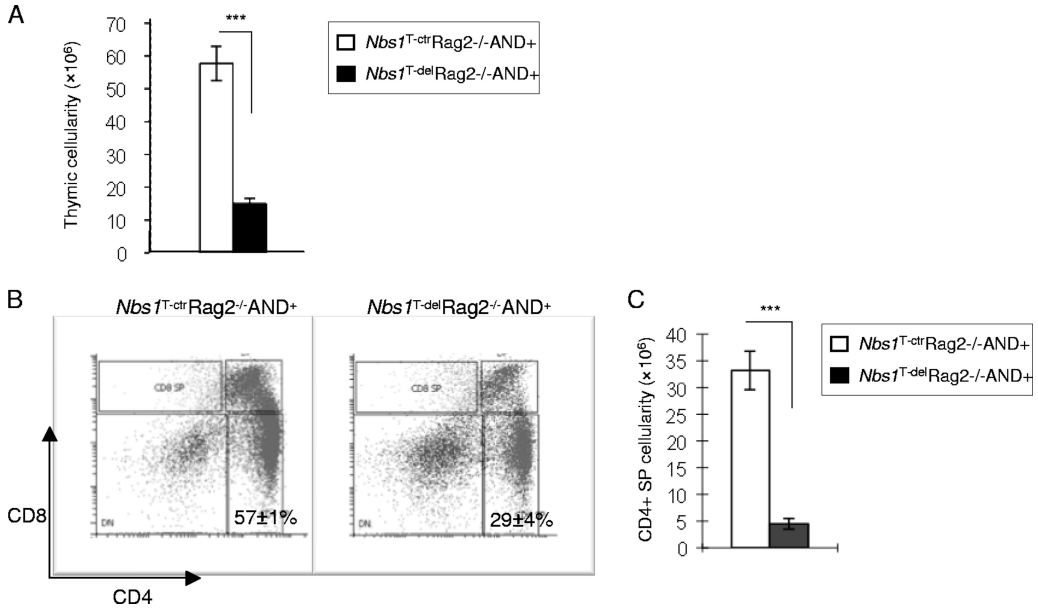

FIG. 7. Rescue experiment of T-cell lymphopenia in *Nbs1*$^{T\text{-}del}$ mice with the TCRαβ transgene (*AND*) and a *Rag2* deficiency. (A) The total thymus cellularity in *Nbs1*$^{T\text{-}ctr}$ *Rag2*$^{-/-}$ *AND*$^{+}$ ($n = 2$) and *Nbs1*$^{T\text{-}del}$ *Rag2*$^{-/-}$ *AND*$^{+}$ ($n = 6$) mice. (B) Representative T-cell profiles of the thymocytes obtained from two *Nbs1*$^{T\text{-}ctr}$ *Rag2*$^{-/-}$ *AND*$^{+}$ mice and four age-matched *Nbs1*$^{T\text{-}del}$ *Rag2*$^{-/-}$ *AND*$^{+}$ mice. (C) The total number of CD4^{+} SP cells obtained from thymi of *Nbs1*$^{T\text{-}del}$ mice ($n = 2$) relative to the controls ($n = 4$) in the *Rag2*$^{-/-}$ *AND*$^{+}$ genetic backgrounds. ***, $P < 0.001$ using Student's unpaired *t* test.

Nbs1-null mice argue that ATM and NBS1 have overlapping, yet distinct, functions in T-cell lymphogenesis.

Interestingly, the blocking of the DN3-DN4 transition is coincident with the TCRβ rearrangement, and the defective V(D)J recombination may be one of the reasons for the severe T-cell lymphopenia in *Nbs1*$^{T\text{-}del}$ mice. Nbs1 is required for a proper coding joint formation because a Nbs1 deletion in particular lengthened the V(D)J joints in the TCRβ locus of *Nbs1*$^{T\text{-}del}$ T cells. The less frequent deletion of the Vβ and Jβ joint regions and the less degraded Dβ1/2 segments might be due to inefficient processing of V(D)J joints in the *Nbs1*$^{T\text{-}del}$ TCRβ locus by Mre11 (the nuclease component of MRN). The MRN complex has the capacities of DNA bridging (by Rad50) and end processing (via the endonuclease and exonuclease activities of Mre11) (4, 43). The persistent DSBs or the defective processing of V(D)J coding ends in the *Nbs1*-null T cells could be due to a defective recruitment of MRN components for DNA end tethering and of DNA end resection factors, such as Mre11, for Rag-generated DSB end processing (44). Consistent with this notion, the binding of Rad50 to the DNA end coding joints in TCRβ as well as in the TCRα locus was attenuated in *Nbs1*-null T cells, thereby compromising the enzymatic activity of Mre11 to process the DNA ends. In addition, the retention of the unrepaired coding joints, suggested by the persistent γ-H2AX signals and open chromatin structure, leaves a broad time window for other terminal modifying enzymes, for example, template-independent TdT, to act on Rag1/2-generated DNA ends, which may account for longer coding joints in the TCRβ locus.

For signal joint formation, which is a direct and fast-joining process of two blunt DNA ends during V(D)J recombination, *Nbs1*$^{T\text{-}del}$ T cells efficiently joined signal ends, consistent with results from other reports (10), suggesting that Nbs1 is dispensable for the joining process. However, it is interesting to notice that the *Nbs1*$^{T\text{-}del}$ T cells signal joints showed a strong preference for the GC-nucleotide insertion, which has not been documented previously in *Nbs1* hypomorphic mutant cells. The mechanism of such a biased use of nucleotides is unclear at the moment, but it is possible that delayed DNA end joining may affect the activity (albeit unintentionally) of the template-independent TdT. Interestingly, the analysis of T cells of Artemis$^{-/-}$ and SCID mice (DNA-PKcs mutated) also revealed an increased bias of GC/AT composition in the signal joints (39). The catalytic activity of TdT could be modified upon binding to DNA-PKcs (31). Previously, the failure of the hairpin opening caused by DNA-PKcs/Artemis in *Atm*$^{-/-}$ T cells indicates that ATM may be involved in the recruitment of DNA-PKcs/Artemis to V(D)J ends (3, 21). It is possible that the impaired MRN-ATM axis in *Nbs1*$^{T\text{-}del}$ T cells may compromise the loading of DNA-PKcs to the DNA ends of signal joints and thus affect the TdT activity and joint sequence diversity.

The severe T-cell lymphopenia in *Nbs1*$^{T\text{-}del}$ mice could also be attributed to increased apoptosis, which may be caused by chromosomal instability. A p53 deficiency relieved the block of DN3-to-DN4 transition and restored the DN4 cell population, indicating that the transition block is likely to be dependent on cell death triggered by persistent DNA coding ends generated during TCRβ V(D)J recombination (Fig. 6A and B). However, in contrast to the neural rescue effect of a p53 deficiency on *Nbs1*-central nervous system (CNS)-deleted mice (14), the p53 deficiency in *Nbs1*$^{T\text{-}del}$ mice did not restore the total thymic cellularity, suggesting that an Nbs1 deletion also has an impact on proliferative expansion in late T-cell development. Since TCRβ expression needs only one round of V(D)J recombination, while TCRα locus expression requires at least five rounds

of V(D)J recombination, a p53 deficiency might be insufficient to rescue those DP cells with extensive unrepaired DNA breaks carrying on during TCRα rearrangements (21, 45).

Another reason for p53's failure to restore the total cellularity is perhaps due to proliferation defects of *Nbs1*$^{\text{T-del}}$ T cells. TCRαβ transgene expression in *Atm*$^{-/-}$ mice could restore up to 80% of the T-cell population (6), suggesting that the V(D)J defect and TCR selection are the major reasons for the T-cell loss in *Atm*$^{-/-}$ mice. Interestingly, when we inhibited the V(D)J-generated DNA breaks by inactivating *Rag2* (36), the TCRαβ transgene partially restored the mature CD4$^+$ T cells in *Nbs1*$^{\text{T-del}}$ mice, which show 51% of controls (1-fold reduction) (Fig. 7B) compared to ~30% of controls (2-fold reduction) (Fig. 2B) in the *Rag2*$^{+/+}$ background. The increased *Nbs1*$^{\text{T-del}}$ CD4$^+$ SP population in the *Rag2*$^{-/-}$ *AND*$^+$ background suggests a role for Nbs1 in the repair of the V(D)J-induced DSBs and perhaps in the positive and negative selection processes. However, even if DSBs are prevented by *Rag2* deficiency and TCRαβ is provided to allow a normal positive and negative selection (in the *Rag2*$^{-/-}$ *AND*$^+$ background), the total CD4$^+$ SP numbers as well as thymic cellularity are still very low in *Nbs1*$^{\text{T-del}}$ *Rag2*$^{-/-}$ *AND*$^+$ mice (Fig. 7A and C). These observations thus well indicate that the function of Nbs1 in cell proliferation is likely to be responsible for the major loss of the T cells in late stages, as suggested previously in Nbs1-deleted B cells (25, 35). Therefore, the loss of T cells after Nbs1 deletion is likely through its function in cell proliferation, viability, and not exclusively, cell death via β selection because of an aberrant V(D)J recombination.

Taken together, a complete deletion of Nbs1 in early T-cell precursors affects TCRβ V(D)J rearrangements and results in the persistence of Rag1/2-generated coding joint ends due to their inefficient processing in the absence of Nbs1. In addition, the *Nbs1*-null mutation abolishes proliferative expansion during positive and negative selection, which cannot be rescued by p53 deletion or overexpression of the TCRαβ transgene. All these mark the common but unique function of Nbs1 (MRN) compared to that of Atm. Thus, the study of T cells devoid of the entire Nbs1 protein reveals a physiological function of Nbs1 in repairing the Rag-induced DSBs during TCRβ recombination and proliferation, and both of which are essential for T-cell development.

ACKNOWLEDGMENTS

We thank Lucien Frappart, Yufeng Liu, and Debra Weih for the histological examinations. We are grateful to Christopher Wilson for providing the Lck-Cre transgenic mice and André Nussenzweig for providing the *Rag2*$^{+/-}$ *AND*$^+$ mice for this study. We also thank Simone Tänzer for cell sorting, Dominique Galendo and Christof Birch-Hirschfeld for their excellent assistance in the maintenance of the animal colonies, and Tjard Jörss for his excellent technical support. We also thank Wanjun Chen and Pierre-Olivier Frappart for their critical reading of the manuscript. Further thanks go to Eileen Stöckl for editing the manuscript. We are also grateful to many other members of our laboratory for helpful discussions.

Z.-Q.W. is supported by the Association for International Cancer Research, United Kingdom, and by the Deutsche Forschungsgemeinschaft, Germany.

REFERENCES

1. **Barlow, C., S. Hirotsune, R. Paylor, M. Liyanage, M. Eckhaus, F. Collins, Y. Shiloh, J. N. Crawley, T. Ried, D. Tagle, and A. Wynshaw-Boris.** 1996. Atm-deficient mice: a paradigm of ataxia telangiectasia. Cell **86:**159–171.
2. **Bassing, C. H., W. Swat, and F. W. Alt.** 2002. The mechanism and regulation of chromosomal V(D)J. recombination. Cell **109:**S45–S55.
3. **Bird, A. W., D. Y. Yu, M. G. Pray-Grant, Q. Qui, K. E. Harmon, P. C. Megee, P. A. Grant, M. M. Smith, and M. F. Christman.** 2002. Acetylation of histone H4 by Esa1 is required for DNA double-strand break repair. Nature **419:** 411–415.
4. **Buis, J., Y. Wu, Y. Deng, J. Leddon, G. Westfield, M. Eckersdorff, J. M. Sekiguchi, S. Chang, and D. O. Ferguson.** 2008. Mre11 nuclease activity has essential roles in DNA repair and genomic stability distinct from ATM activation. Cell **135:**85–96.
5. **Candeias, S., K. Muegge, and S. K. Durum.** 1996. Junctional diversity in signal joints from T cell receptor beta and delta loci via terminal deoxynucleotidyl transferase and exonucleolytic activity. J. Exp. Med. **184:**1919–1926.
6. **Chao, C., E. M. Yang, and Y. Xu.** 2000. Rescue of defective T cell development and function in Atm$^{-/-}$ mice by a functional TCR alpha beta transgene. J. Immunol. **164:**345–349.
7. **Chen, H. T., A. Bhandoola, M. J. Difilippantonio, J. Zhu, M. J. Brown, X. Tai, E. P. Rogakou, T. M. Brotz, W. M. Bonner, T. Ried, and A. Nussenzweig.** 2000. Response to RAG-mediated V(D)J cleavage by NBS1 and γ-H2AX. Nature **290:**1962–1964.
8. **Corneo, B., R. L. Wendland, L. Deriano, X. Cui, I. A. Klein, S. Y. Wong, S. Arnal, A. J. Holub, G. R. Weller, B. A. Pancake, S. Shah, V. L. Brandt, K. Meek, and D. B. Roth.** 2007. Rag mutations reveal robust alternative end joining. Nature **449:**483–486.
9. **D'Amours, D., and S. P. Jackson.** 2002. The Mre11 complex: at the crossroads of DNA repair and checkpoint signalling. Nat. Rev. Mol. Cell Biol. **3:**317–327.
10. **Deriano, L., T. H. Stracker, A. Baker, J. H. Petrini, and D. B. Roth.** 2009. Roles for NBS1 in alternative nonhomologous end-joining of V(D)J recombination intermediates. Mol. Cell **34:**13–25.
11. **Digweed, M., and K. Sperling.** 2004. Nijmegen breakage syndrome: clinical manifestation of defective response to DNA double-strand breaks. DNA Repair (Amst.) **3:**1207–1217.
12. **Dinkelmann, M., E. Spehalski, T. Stoneham, J. Buis, Y. Wu, J. M. Sekiguchi, and D. O. Ferguson.** 2009. Multiple functions of MRN in end-joining pathways during isotype class switching. Nat. Struct. Mol. Biol. **16:**808–813.
13. **Dudley, D. D., J. Chaudhuri, C. H. Bassing, and F. W. Alt.** 2005. Mechanism and control of V(D)J recombination versus class switch recombination: similarities and differences. Adv. Immunol. **86:**43–112.
14. **Frappart, P. O., W. M. Tong, I. Demuth, I. Radovanovic, Z. Herceg, A. Aguzzi, M. Digweed, and Z. Q. Wang.** 2005. An essential function for NBS1 in the prevention of ataxia and cerebellar defects. Nat. Med. 474–475.
15. **Harfst, E., S. Cooper, S. Neubauer, L. Distel, and U. Grawunder.** 2000. Normal V(D)J recombination in cells from patients with Nijmegen breakage syndrome. Mol. Immunol. **37:**915–929.
16. **Hayday, A. C., and D. J. Pennington.** 2007. Key factor in the organized chaos of early T cell development. Nat. Immunol. **8:**137–144.
17. **Helmink, B. A., A. L. Bredemeyer, B. S. Lee, C. Y. Huang, G. G. Sharma, L. M. Walker, J. J. Bednarski, W. L. Lee, T. K. Pandita, C. H. Bassing, and B. P. Sleckman.** 2009. MRN complex function in the repair of chromosomal Rag-mediated DNA double-strand breaks. J. Exp. Med. **206:**669–679.
18. **Herceg, Z., H. Li, C. Cuenin, V. Shukla, M. Radolf, P. Steinlein, and Z. Q. Wang.** 2003. Genome-wide analysis of gene expression regulated by the HAT cofactor Trrap in conditional knockout cells. Nucleic Acids Res. **31:**7011–7023.
19. **Hopfner, K. P., L. Craig, G. Moncalian, R. A. Zinkel, T. Usui, B. A. Owen, A. Karcher, B. Henderson, J. L. Bodmer, C. T. McMurray, J. P. Carney, J. H. Petrini, and J. A. Tainer.** 2002. The Rad50 zinc-hook is a structure joining Mre11 complexes in DNA recombination and repair. Nature **418:**562–566.
20. **Hsieh, C. L., C. F. Arlett, and M. R. Lieber.** 1993. V(D)J recombination in ataxia telangiectasia, Bloom's syndrome, and a DNA ligase I-associated immunodeficiency disorder. J. Biol. Chem. **268:**20105–20109.
21. **Huang, C. Y., G. G. Sharma, L. M. Walker, C. H. Bassing, T. K. Pandita, and B. P. Sleckman.** 2007. Defects in coding joint formation in vivo in developing ATM-deficient B and T lymphocytes. J. Exp. Med. **204:**1371–1381.
22. **International Nijmegen Breakage Syndrome Study Group.** 2000. Nijmegen breakage syndrome. Arch. Dis. Child. **82:**400–406.
23. **Kang, J., R. T. Bronson, and Y. Xu.** 2002. Targeted disruption of NBS1 reveals its roles in mouse development and DNA repair. EMBO J. **21:**1447–1455.
24. **Kaye, J., M. L. Hsu, M. E. Sauron, S. C. Jameson, N. R. Gascoigne, and S. M. Hedrick.** 1989. Selective development of CD4$^+$ T cells in transgenic mice expressing a class II MHC-restricted antigen receptor. Nature **341:**746–749.
25. **Kracker, S., Y. Bergmann, I. Demuth, P. O. Frappart, G. Hildebrand, R. Christine, Z.-Q. Wang, K. Sperling, M. Digweed, and A. Radbruch.** 2005. Nibrin functions in Ig class-switch recombination. Proc. Natl. Acad. Sci. U. S. A. **102:**1584–1589.
26. **Lavin.** 2007. ATM and the Mre11 complex combine to recognize and signal DNA double-strand breaks. Oncogene **26:**7749–7758.
27. **Lee, J. H., and T. T. Paull.** 2005. ATM activation by DNA double-strand breaks through the Mre11-Rad50-Nbs1 complex. Science **308:**551–554.

28. **Lieber, M. R.** 2010. The mechanism of double-strand DNA break repair by the nonhomologous DNA end-joining pathway. Annu. Rev. Biochem. **79:** 181–211.
29. **Lyons, A. B., J. Hasbold, and P. D. Hodgkin.** 2001. Flow cytometry analysis of cell division history using dilution of carboxyfluorescein diacetate succinimidyl ester, a stably integrated fluorescent probe. Methods Cell Biol. **63:**375–398.
30. **Michalkiewicz, J., C. Barth, K. Chrzanowska, H. Gregorek, M. Syczewska, C. M. B. Weemaes, K. Madalinski, D. Dzierzanowska, and J. Stachowski.** 2003. Abnormalities in the T and NK lymphocyte phenotype in patients with Nijmegen breakage syndrome. Clin. Exp. Immunol. **134:**482–490.
31. **Mickelsen, S., C. Snyder, K. Trujillo, M. Bogue, D. B. Roth, and K. Meek.** 1999. Modulation of terminal deoxynucleotidyltransferase activity by the DNA-dependent protein kinase. J. Immunol. **163:**834–843.
32. **Paull, T. T., and M. Gellert.** 1998. The 3′ to 5′ exonuclease activity of Mre11 facilitates repair of DNA double-strand breaks. Mol. Cell **1:**969–979.
33. **Qi, L., M. A. Strong, B. O. Karim, M. Armanios, D. L. Huso, and C. W. Greider.** 2003. Short telomeres and ataxia-telangiectasia mutated deficiency cooperatively increase telomere dysfunction and suppress tumorigenesis. Cancer Res. **63:**8188–8196.
34. **Rass, E., A. Grabarz, I. Plo, J. Gautier, P. Bertrand, and B. S. Lopez.** 2009. Role of Mre11 in chromosomal nonhomologous end joining in mammalian cells. Nat. Struct. Mol. Biol. **16:**819–824.
35. **Reina-San-Martin, B., M. C. Nussenzweig, A. Nussenzweig, and S. Difilippantonio.** 2005. Genomic instability, endoreduplication, and diminished Ig class-switch recombination in B cells lacking Nbs1. Proc. Natl. Acad. Sci. U. S. A. **102:**1590–1595.
36. **Shinkai, Y., G. Rathbun, K. P. Lam, E. M. Oltz, V. Stewart, M. Mendelsohn, J. Charron, M. Datta, F. Young, A. M. Stall, et al.** 1992. RAG-2-deficient mice lack mature lymphocytes owing to inability to initiate V(D)J rearrangement. Cell **68:**855–867.
37. **Stucki, M., and S. P. Jackson.** 2006. gammaH2AX and MDC1: anchoring the DNA-damage-response machinery to broken chromosomes. DNA Repair (Amst.) **5:**534–543.
38. **Touvrey, C., E. Borel, P. N. Marche, E. Jouvin-Marche, and S. M. Candeias.** 2006. Gene-specific signal joint modifications during V(D)J recombination of TCRAD locus genes in murine and human thymocytes. Immunobiology **211:**741–751.
39. **Touvrey, C., C. Couedel, P. Soulas, R. Couderc, M. Jasin, J. P. de Villartay, P. N. Marche, E. Jouvin-Marche, and S. M. Candeias.** 2008. Distinct effects of DNA-PKcs and Artemis inactivation on signal joint formation in vivo. Mol. Immunol. **45:**3383–3391.
40. **Uziel, T., Y. Lerenthal, L. Moyal, Y. Andegeko, L. Mittelman, and Y. Shiloh.** 2003. Requirement of the MRN complex for ATM activation by DNA damage. EMBO J. **22:**5612–5621.
41. **Vacchio, M. S., A. Olaru, F. Livak, and R. J. Hodes.** 2007. ATM deficiency impairs thymocyte maturation because of defective resolution of T cell receptor alpha locus coding end breaks. Proc. Natl. Acad. Sci. U. S. A. **104:** 6323–6328.
42. **Weemaes, C. M., D. F. Smeets, and C. J. van der Burgt.** 1994. Nijmegen breakage syndrome: a progress report. Int. J. Radiat. Biol. **66:**S185–S188.
43. **Williams, R. S., G. Moncalian, J. S. Williams, Y. Yamada, O. Limbo, D. S. Shin, L. M. Groocock, D. Cahill, C. Hitomi, G. Guenther, D. Moiani, J. P. Carney, P. Russell, and J. A. Tainer.** 2008. Mre11 dimers coordinate DNA end bridging and nuclease processing in double-strand-break repair. Cell **135:**97–109.
44. **Xie, A., A. Kwok, and R. Scully.** 2009. Role of mammalian Mre11 in classical and alternative nonhomologous end joining. Nat. Struct. Mol. Biol. **16:**814–818.
45. **Xu, Y., E. M. Yang, J. Brugarolas, T. Jacks, and D. Baltimore.** 1998. Involvement of p53 and p21 in cellular defects and tumorigenesis in $Atm^{-/-}$ mice. Mol. Cell. Biol. **18:**4385–4390.
46. **Yan, C. T., C. Boboila, E. K. Souza, S. Franco, T. R. Hickernell, M. Murphy, S. Gumaste, M. Geyer, A. A. Zarrin, J. P. Manis, K. Rajewsky, and F. W. Alt.** 2007. IgH class switching and translocations use a robust non-classical end-joining pathway. Nature **449:**478–482.
47. **Yang, Y. G., A. Saidi, P. O. Frappart, W. Min, C. Barrucand, V. Dumon-Jones, J. Michelon, Z. Herceg, and Z. Q. Wang.** 2006. Conditional deletion of Nbs1 in murine cells reveals its role in branching repair pathways of DNA double-strand breaks. EMBO J. **25:**5527–5538.
48. **Yeo, T. C., D. Xia, S. Hassouneh, X. O. Yang, D. E. Sabath, K. Sperling, R. A. Gatti, P. Concannon, and D. M. Willerford.** 2000. V(D)J rearrangement in Nijmegen breakage syndrome. Mol. Immunol. **37:**1131–1139.
49. **Zhang, Y., J. Zhou, and C. U. Lim.** 2006. The role of NBS1 in DNA double strand break repair, telomere stability, and cell cycle checkpoint control. Cell Res. **16:**45–54.